Acta Biomaterialia 85 (2019) 310–319

Contents lists available at ScienceDirect

Acta Biomaterialia

journal homepage: www.elsevier.com/locate/actabiomat

Full length article

Molecularly engineered metal-based bioactive soft materials – Neuroactive magnesium ion/polymer hybrids

Lijie Sun [a], Min Wang [a], Shuo Chen [a], Binbin Sun [b], Yifan Guo [a], Chuanglong He [b], Xiumei Mo [b], Bo Zhu [c], Zhengwei You [a,*]

[a] State Key Laboratory for Modification of Chemical Fiber and Polymer Materials, International Joint Laboratory for Advanced Fiber and Low-dimension Materials, College of Materials Science and Engineering, Donghua University, North Renmin Road 2999, Shanghai 201620, China
[b] College of Chemistry, Chemical Engineering and Biotechnology, Donghua University, North Renmin Road 2999, Shanghai 201620, China
[c] School of Materials Science & Engineering, Shanghai University, Shanghai 200444, China

ARTICLE INFO

Article history:
Received 3 September 2018
Received in revised form 13 December 2018
Accepted 21 December 2018
Available online 23 December 2018

Keywords:
Metal ion
Polymer hybrid
Poly(glycerol-sebacate)
Controlled release
Schwann cells
Soft biomaterials

ABSTRACT

The development of bioactive soft materials that can guide cell behavior and have biomimetic mechanical properties is an active and challenging topic in regenerative medicine. A common strategy to create a bioactive soft material is the integration of biomacromolecules with polymers. However, limited by their complex structures and sensitivity to temperature and chemicals, it is relatively difficult to maintain the bioactivity of biomacromolecules during their preparation, storage, and application. Here, a new kind of bioactive soft material based on the molecular integration of metal ions and polymers is designed and exemplified by a hybrid of magnesium ion (Mg^{2+}) and poly(glycerol-sebacate-maleate) (PGSM-Mg). Mg^{2+} was firmly incorporated into PGSM molecules through a complexation interaction as evidenced by X-ray photoelectron spectroscopy (XPS) and Fourier-transform infrared spectroscopy (FTIR). The PGSM matrix provided the soft nature and facile processing of the hybrid, which could serve as an injectable material and be fabricated into elastic porous three-dimensional (3D) scaffolds. The Mg^{2+} immobilized in the PGSM chain conferred neuroactivity to the resultant hybrid. PGSM-Mg exhibited adequate biodegradability and a sustained release of Mg^{2+}. PGSM-Mg 3D scaffolds promoted the adhesion and proliferation of Schwann cells (SCs) more effectively than poly(lactic-*co*-glycolic acid) (PLGA) scaffolds. Furthermore, SCs on PGSM-Mg scaffolds expressed significantly more neural specific genes than those on PLGA, PGS, and PGSM, including nerve growth factor (NGF) and neurotrophic factor-3 (NTF3). All these results indicated that Mg^{2+} immobilized through molecular integration could efficiently regulate the bioactivity of polymers. In view of the wide availability, diverse bioactivity, and high stability of metal ions, the strategy of molecular coupling of metal ions and polymers is expected to be a new general approach to construct bioactive soft materials.

Statement of Significance

Bioactive soft materials are designed on the basis of the molecular integration of metal ions and polymers. Immobilized metal ions offer a new way to endow bioactivity to polymers. Different from biomolecules such as proteins and genes, metal ions are quite stable and can resist harsh processing conditions. Further, the polymeric matrix provides the soft nature and facile processing of the hybrid. Different from stiff metal-containing inorganic materials, the hybrid is a biomimetic soft material and can be readily processed just like its polymer precursor under mild conditions. In view of the diversity of metal ions and polymers, this strategy is expected to be a new powerful and general approach to construct bioactive soft materials for a wide range of biomedical applications.

1. Introduction

Synthetic polymers play an increasingly important role in widely used biomedical devices and emerging regenerative

* Corresponding author.
E-mail address: zyou@dhu.edu.cn (Z. You).

https://doi.org/10.1016/j.actbio.2018.12.040
1742-7061/

medicine because of its widely available composition and architectures, controllable and reproducible structures, diverse and tunable properties, easy purification and processing, and low risks of immunogenicity and disease transmission [1–3]. Bioactivity is a major direction of new-generation biomaterials [4]. However, most synthetic polymers are biologically inert and cannot achieve effectively biological communication. Therefore, bio-functionalization of polymers is of great significance [5]. A common strategy to create bioactive polymers is the integration of biomacromolecules such as proteins [6,7], genes[8,9], and their subunits [10,11]. However, owing to their complex structures and sensitivity to temperature and chemicals, it is relatively difficult to maintain the bioactivity of biomacromolecules during their preparation, storage, and application.

Metal ions play important roles in various biological processes. It is well established that a number of metal ions (such as Mg^{2+}, Zn^{2+}, and Fe^{2+}) are essential to life, participate in many biological reactions (such as RNA and DNA in protein synthesis), and regulate biological activity (enzyme activation and inflammatory response) [12–14]. In recent years, increasing evidence in literature indicates that the integration of metal ions into materials can provide important biological cues to effectively promote cell adhesion, proliferation, differentiation, and even *in vivo* regeneration process [15–18]. Therefore, the use of bioactive metal ions instead of complex biomacromolecules to control the bioactivity processes makes them a great potential candidate for biomedical applications. However, most studies on integrating metal ions into biomaterials are based on inorganic materials, which are usually applied for hard tissues but not suitable for soft tissue applications owing to their stiff nature [19–21].

Here, we reason that incorporating metal ions into polymers through molecular integration is a promising strategy to produce bioactive soft materials for various biomedical applications, especially for soft tissues. Metal ions usually have high thermal and chemical stability, and hence, they are compatible to various processes of polymers and easily integrate with various polymers. Thus, metal ions provide a much more facile and efficient way than complex biomacromolecules to modulate the bioactivity of diverse polymers. Despite their great potential for biomedical applications, studies on metal ions/polymers hybrids are limited. Some previous reports showed composite scaffolds or hydrogels prepared by physical blending of polymers with metal or metallic oxide nanoparticles [18,22]. However, owing to the difficulty in the dispersion of nanoparticles, it is difficult to obtain uniform composites. In addition, few studies used metal ions as crosslinkers to synthesize natural polymer-based hydrogels [23]. Nevertheless, the distribution of metal ions in hydrogels was usually inhomogeneous because of uncontrolled crosslinking, and the influence of metal ions on cell behavior had not been well studied [23].

As a proof of principle, herein, we designed a novel Mg^{2+}/polymer hybrid, PGSM-Mg, and demonstrated its ability to promote the expression of nerve growth factor (NGF) and neurotrophic factor-3 (NTF3) of SCs (Fig. 1). The design is based on the following considerations: (i) Poly(glycerol sebacate) (PGS) was selected as the polymeric backbone. PGS has been widely used to regenerate soft tissues including the nerve [24–28] owing to its excellent biocompatibility, biodegradability, and biomimetic mechanical properties [29]. Furthermore, PGS has extensive hydroxyl groups, which provided a great potential for postmodification including incorporation of metal ions. (ii) Magnesium ion (Mg^{2+}) was selected as the model metal ion. Mg^{2+} was found to play a vital role in the repair or regeneration of peripheral nerve [30,31]. Particularly, it could induce SCs to secrete NGF and promote the regeneration of nerve axons [31,32]. Thus, the Mg^{2+}/polymer hybrid may be neuroactive. (iii) The carboxyl group was selected as the molecular bridge between PGS and metal ions. This group is widely distributed in living organisms and one of the most common groups that bind metal ions in the body [13]. Herein, we used a biocompatible maleic acid unit to readily attach carboxyl groups to the pendent hydroxyl groups of PGS in one step [33]. The concise synthesis would enable the wide availability of resultant hybrid materials.

2. Materials and methods

2.1. Materials and reagents

Sebacic acid and anhydrous N,N-dimethyl formamide (DMF) were purchased from J&K. Sebacic acid was recrystallized from anhydrous ethanol three times. Anhydrous glycerol was provided by Sigma-Aldrich. Maleic anhydride, magnesium chloride hexahydrate ($MgCl_2{\cdot}6H_2O$), and organic solvents were all obtained from

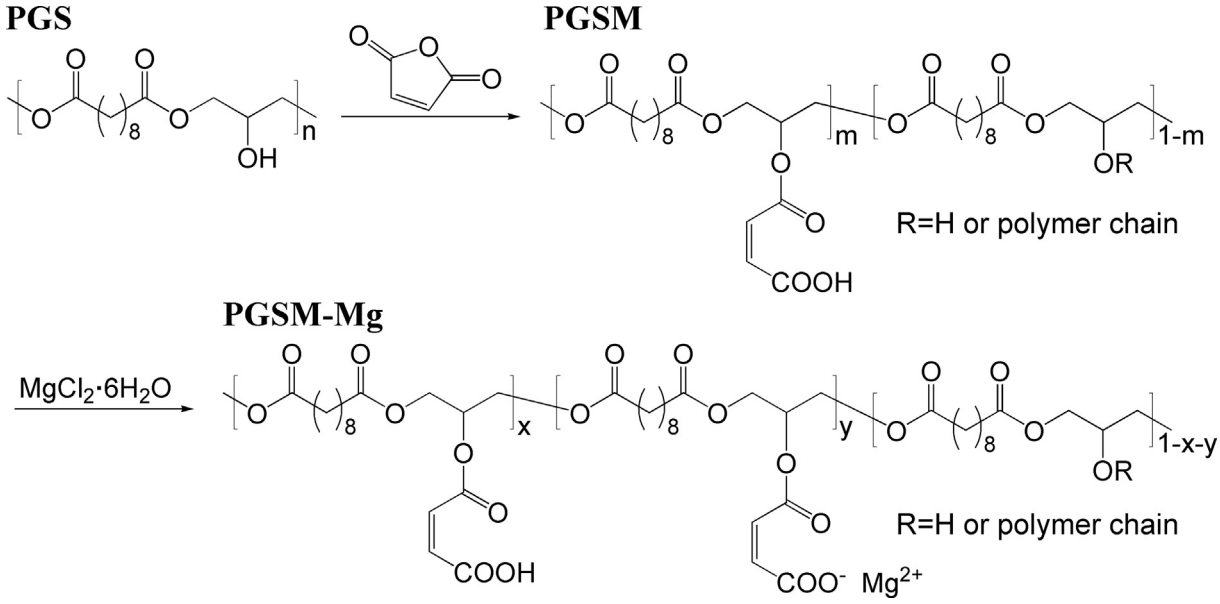

Fig. 1. Design and synthesis of PGSM-Mg. PGSM can be gained by PGS and maleic anhydride without any catalyst. The free carboxyl group can easily bind Mg^{2+}, which serves as a neuroactive factor.

Sinopharm Chemical Reagent Co., Ltd., and used without further purification.

2.2. Synthesis of PGS

PGS was synthesized according to a previous report [29]. The equimolar amounts of recrystallized sebacic acid and anhydrous glycerol were added to a 500-mL three-neck flask. The reactants were steadily heated to 135 °C and bubbling N_2 was passed through a bubbler. The mixture was stirred at 135 °C for 24 h before the N_2 bubbler was removed and vacuum was applied. The reaction mixture was stirred continuously at 1 Torr and 135 °C for another 24 h. The resultant polymer was a pale yellow, highly viscous semi-solid.

2.3. Synthesis of PGSM

Maleic anhydride (2 equivalents based on the theoretical molar amount of hydroxyl groups in PGS) was added to an anhydrous DMF solution of PGS under a nitrogen atmosphere at 110 °C. The mixture was stirred at 110 °C for 50 min. Then, it was quenched with deionized water and concentrated on an evaporator. The raw product was redissolved in THF, precipitated in deionized water, and lyophilized under vacuum at room temperature to yield PGSM.

2.4. Synthesis of PGSM-Mg

An equivalent molar amount of PGSM and $MgCl_2{\cdot}6H_2O$ was mixed and dissolved in acetone in a round-bottom flask. The mixture was stirred at 60 °C for 24 h. Then, it was quenched with deionized water and concentrated on an evaporator. The raw product was redissolved in acetone, precipitated in deionized water, and lyophilized under vacuum at room temperature to yield PGSM-Mg as a faint yellow semi-solid.

2.5. Fabrication of scaffolds

Porous scaffolds of PGS, PGSM, and PGSM-Mg were prepared by a modified salt fusion method [34]. The process is briefly described below. Salt particles with a size range of 75–150 μm were placed into a mold consisting of three components: a Teflon-coated stainless-steel disk, a Teflon-coated ring-shaped steel shim, and permanent magnets to join the assembly. The thickness of the final scaffold was 1 mm and was controlled by the corresponding shim. The molds were transferred to and kept in a humidity chamber at 37 °C and 85% relative humidity for 1.5 h. The fused salt templates were dried in an oven at 120 °C for 1.5 h. The aforementioned PGSM-Mg reaction mixture in acetone was added to the salt mold. The acetone was allowed to evaporate in a fume hood for 30 min. The mold was transferred to a vacuum oven and cured at 150 °C under 1 Torr for 24 h. The resultant PGSM-Mg-impregnated salt template was soaked in deionized water at room temperature for 24 h, with the water changed every 6 h. Then, the scaffold was lyophilized.

2.6. Characterization and measurement

The molecular weights and their distributions in polymers were determined by Waters gel permeation chromatography (GPC) (Malvern TDAmax, USA) with a differential refractive index detector and a Brookhaven multi-angle light scattering detector. The measurement was performed at 40 °C using THF (HPLC grade) as the eluent. The ^{1}H NMR spectrum was recorded on a Bruker AVANCE 400 NMR. The surface compositions of the PGSM and PGSM-Mg were determined using an X-ray photoelectron spectrometer (XPS; Thermo ESCALAB 250X) with a monochromatized Al Kα source (1486.6 eV). All binding energies were normalized with the C1s (284.6 eV) peak of the contamination carbon as an internal standard. The attenuated total reflectance-Fourier-transform infrared (ATR-FTIR) spectra were recorded on a Thermo Scientific Nicolet 6700 spectrometer. Inductively coupled plasma atomic emission spectra (ICP-AES) were recorded on a Leeman Prodigy ICP spectrometer. The samples were degraded with nitric acid before the ICP test. For the measurement of static air–water contact angles, glass slides were coated with an acetone solution of PGSM and PGSM-Mg. The glass slides were dried at room temperature under 1 Torr for 24 h after the solvent was evaporated in air to produce thin films of PGSM and PGSM-Mg. Then, the static air–water contact angles of the films were recorded on a contact angle instrument (Contact Angle System OCA 40, Dataphysics Co., Germany) at room temperature. Ten measurements were made and averaged for each sample. Thermogravimetric analyses (TGA) of PGS, PGSM, and PGSM-Mg were conducted on a Discovery TGA (TA, USA) from 40 °C to 600 °C at a heating rate of 10 °C min^{-1} under nitrogen atmosphere. Differential scanning calorimetry (DSC) was conducted on a NETZSCH DSC 204 F1 Phoenix from −70 °C and 150 °C at a heating rate of 10 °C min^{-1} under nitrogen atmosphere. The glass transition temperature (T_g) was defined as the midpoint of the glass transition and determined using NETZSCH. Rheology tests were carried out on a rotational rheometer (RS 150, Haake Co., Germany), with a shear rate from 0 to 50 s^{-1} at different temperatures. Morphology of the sample and magnesium distribution in it were characterized using a field-emission scanning electron microscope (FE-SEM; HITACHI SU-8010, Japan) and energy-dispersive X-ray spectroscopy (Oxford Inca X-Max, UK) with an acceleration voltage of 1 or 15 kV and an emission current of 10 μA, respectively.

2.7. Mg^{2+} release of PGSM-Mg film and scaffold

The tetrahydrofuran solution of PGSM-Mg (100 mg mL^{-1}, 80 μL) was dropped into cylinder-shaped bottles with an inner diameter of 20 mm and then dried at room temperature under 1 Torr for 48 h after solvent evaporation in air to produce a thin film of the PGSM-Mg film. In addition, disk-shaped PGSM-Mg scaffolds (9.38 mm in diameter by 1 mm thickness) were used directly. An *in vitro* release test was performed in phosphate-buffered saline (PBS). Then, at each time point, 6 mL of PBS was taken out and 6 mL of fresh PBS was added back. The release of Mg^{2+} was determined using a Leeman Prodigy ICP spectrometer. The values of three samples were averaged.

2.8. Mechanical properties of the PGSM-Mg scaffold

The mechanical properties of the PGS, PGSM, and PGSM-Mg scaffolds were evaluated by compression tests using an Instron 5969 universal testing machine with a 5 N sensor. Disk-shaped specimens (11.5 mm in diameter by 4 mm thickness) were punched from the PGSM-Mg scaffold. Each specimen was compressed to a strain of 40% at a rate of 1.00 mm min^{-1} with an initial load of 0.01 N. The compression modulus was calculated by taking the initial slope of the stress–strain curve. The data from 5 specimens were averaged for each sample. In the cyclic compression test, the specimens were compressed to a strain of 40% and then allowed to recover to 5% before immediately compressing to a strain of 40% at a rate of 1.00 mm min^{-1} for 4 times.

2.9. In vitro degradation of the PGSM-Mg scaffold

An *in vitro* degradation test was performed in PBS. Disk-shaped samples (9.38 mm in diameter by 1 mm thickness) were weighed

and placed in the PBS solution (6 mL per sample) and incubated at 37 °C. To maintain the concentration of the solution, 6 mL of PBS was taken out and 6 mL of fresh PBS was added back every 7 days. Samples were retrieved, washed with deionized water, lyophilized, and weighted every 7 days. The degree of degradation was determined by dry weight change. Three replicates were performed and the values averaged.

2.10. Material–SC interaction

2.10.1. Preparation of polymer surfaces for cell culture

PGSM-Mg was coated on tissue culture-treated polystyrene (TCPS) surfaces as follows. A 2,2,2-trifluoroethanol solution of polymer (1 g L^{-1}) was filtered through a 0.2 μm filter and added to 24-well (80 μL per well) or 96-well (20 μL per well) TCPS plates. The plates were dried under vacuum overnight after solvent evaporation in air, sterilized with UV light for 12 h, and washed with PBS (3 × 1 mL per well for a 24-well plate, 3 × 100 μL per well for 96-well plate) and culture medium (1 × 500 μL per well for 24-well plate and 1 × 100 μL per well for 96-well plate) with gentle shaking before use. PLGA, PGS, and PGSM coating on TCPS surfaces were used as controls and prepared in the same manner as that of the PGSM-Mg coating.

2.10.2. Cell culture

Wallerian-degenerated sciatic nerves were harvested from adult rats. Schwann cells (SCs) were cultured by enzymatic digestion and differential adhesion methods. SCs were cultured in 89% Dulbecco's Modified Eagle's Medium (DMEM, high glucose) (~19.2 mg L^{-1} Mg^{2+}) supplemented with 10% fetal bovine serum (FBS) (~23.1 mg L^{-1} Mg^{2+}) and 1% penicillin–streptomycin formulation in a fully humidified incubator (37 °C, 5% CO_2). The culture medium was changed 1 day after isolation and every subsequent third day. Within approximately 5–7 days, cells reached subconfluency and were passaged. Passage 2 SCs were used for all cell function tests.

2.10.3. Cell morphology

SCs single-cell suspensions (500 cells per well) were cultured on TCPS, PLGA, PGS, PGSM, and PGSM-Mg surfaces in 96-well plates in a humidified incubator. SC images were captured to observe the cytoskeletal structure after seeding for 4 days and 6 days using an inverted microscope (Olympus IX-71, Japan).

2.10.4. Cell proliferation

To investigate the effect of PGSM-Mg on the proliferation of SCs, CCK-8 assay was performed. SCs were seeded on TCPS, PLGA, PGS, PGSM, and PGSM-Mg surfaces for 2, 4, 6, and 8 days in 96-well plates (500 cells per well, n = 8 per surface per time point). At each time point, 3 μL of the CCK-8 solution was added to each of the 96 wells. After culturing for 3.5 h in a fully humidified incubator (37 °C, 5% CO_2), the absorbance at a wavelength of 450 nm was measured by a SynergyMX plate reader (Biotek, Winooski, VT).

2.10.5. Real-time quantitative PCR (RT-qPCR) analysis for neural-specific gene expression of SCs

The effect of PGSM-Mg on SC neural-specific gene expression was assessed by RT-qPCR to measure the mRNA expression of NGF in all groups after 6 days of culture. Total RNA was extracted using Trizol Reagent (Invitrogen, Life Technologies). Complementary DNA was synthesized from 1 μg of total RNA using RevertAid First Strand cDNA Synthesis Kit (Thermo Fisher Scientific) following the manufacturer's protocol. The RT-qPCR primers were designed based on cDNA sequences from the NCBI Sequence database, and the primer specificity was confirmed by BLASTN searches. RT-qPCR was performed on the ABI Prism 7300 Sequence Detection System (Applied Biosystems, Australia) using FastStart Universal SYBR Green Master (Rox) reagent (Roche). In brief, cDNA samples (2.5 μL of 1:10 diluted template for a total volume of 25 μL per reaction) were analyzed for the gene of interest and the reference gene glyceraldehyde-3-phosphate-dehydrogenase (GAPDH). All experimental samples were run in triplicate for three independent experiments. Dissociation curve analysis was performed to validate the absence of primer dimers and nonspecific PCR products. The mean cycle threshold (Ct) value of each target gene was normalized against the Ct value of GAPDH and the relative expression calculated using the following formula: $2^{-(\text{normalized average Cts})} \times 10^4$.

2.11. Material-SC interaction on 3D scaffolds

2.11.1. Cell culture on polymer 3D scaffolds

The disk-shaped scaffolds (diameter: 4.5 mm for 96-well plates and 34.8 mm for 6-well plates, thickness: 1 mm) were punched from porous polymer sheets. After autoclaving, the scaffolds were progressively soaked in 70%, 50%, and 25% ethanol, as well as PBS for 30 min each with gentle shaking on an orbital shaker. Then, the scaffolds were washed with PBS again and preconditioned overnight in cell culture medium. The scaffolds were transferred to 96-well and 6-well plates, and the residual culture medium was removed by vacuum. SCs were cultured in 89% DMEM (high glucose) supplemented with 10% FBS and 1% penicillin–streptomycin formulation in a fully humidified incubator (37 °C, 5% CO_2). The culture medium was changed every 2 days.

2.11.2. Live/dead staining assay

Briefly, after sterilization with UV light for 1 h, the PLGA, PGS, PGSM, and PGSM-Mg scaffolds were fixed at the bottom of the 24-well plate, and then SCs were seeded on these films at a density of 5000 cells cm^{-2}. After cultured for 8 days, cells on each films were washed with PBS three times and treated with propidium iodide (PI, 0.5 μM) and calcein AM (0.25 μM) (Live/Dead Viability Kit; Molecular Probes) for 45 min. Cells were observed under an inverted fluorescence microscope (Olympus IX-71, Japan).

2.11.3. Scanning electron microscopy

The morphology of the constructs was investigated by SEM. SCs were seeded on 24-well TCPS plates. After 8 days, the phase contrast images were captured on the inverted microscope Eclipse Ti (Nikon, Melville, NY) with a RETIGA-SRV digital camera (QImaging, BC, Canada).

2.11.4. Cell proliferation on 3D scaffold

To investigate the effect of PGSM-Mg scaffolds on the proliferation of SCs, CCK-8 assay was performed. SCs were seeded on PLGA, PGS, PGSM, and PGSM-Mg scaffolds for 2, 4, 6, and 8 days in 96-well plates (500 cells per well, n = 6 per surface per time point). At each time point, 3 μL of the CCK-8 solution was added to each of the 96 wells. After culturing for 3.5 h in a fully humidified incubator (37 °C, 5% CO_2), the absorbance at a wavelength of 450 nm was measured using a SynergyMX plate reader (BioTek, Winooski, VT).

2.11.5. Real-time quantitative PCR (RT-qPCR) analysis for neural-specific gene expression of SCs

The effect of PGSM-Mg scaffolds on SC neural-specific gene expression was assessed by RT-qPCR to measure the mRNA expression of NGF and NTF3 in all groups after 6 days of culture. Total RNA was extracted using Trizol Reagent (Invitrogen, Life Technologies). Complementary DNA was synthesized from 1 μg of total RNA using RevertAid First Strand cDNA Synthesis Kit (Thermo Fisher Scientific) following the manufacturer's protocol. The RT-qPCR

primers were designed depending on cDNA sequences from the NCBI Sequence database, and the primer specificity was confirmed by BLASTN searches. RT-qPCR was performed on the ABI Prism 7300 Sequence Detection System (Applied Biosystems, Australia) using FastStart Universal SYBR Green Master (Rox) reagent (Roche). In brief, cDNA samples (2.5 μL of 1:10 diluted template for a total volume of 25 μL per reaction) were analyzed for the gene of interest and the reference gene glyceraldehyde-3-phosphate-dehydrogenase (GAPDH). All experimental samples were run in triplicate for three independent experiments. Dissociation curve analysis was performed to validate the absence of primer dimers and nonspecific PCR products. The mean cycle threshold (Ct) value of each target gene was normalized against the Ct value of GAPDH and the relative expression calculated using the following formula: $2^{-(\text{normalized average Cts})} \times 10^4$.

2.12. Statistical analysis

Statistical analysis was performed using one-way ANOVA and LSD *post hoc* multiple comparison with a minimum confidence level of $p < 0.05$ for statistical significance. All values are reported as the mean ± standard deviation.

3. Results

3.1. Synthesis and characterization of PGSM-Mg

PGS with a number average molecular weight (M_n) of 21.3 kDa and a polydispersity index (PDI) of 3.2 was synthesized by polycondensation between glycerol and sebacic acid according to previous reports [35]. PGS reacted with maleic anhydride to produce PGSM with a M_n of 37.6 kDa and a PDI of 2.9. The structure of PGSM was confirmed by ^{1}H NMR (Fig. S1). PGSM-Mg was prepared by an exchange reaction between PGSM and $MgCl_2$ (Fig. 1). The crude product was extensively washed with water to remove physically absorbed Mg^{2+}. For comparison, $MgCl_2$ was directly reacted with unmodified PGS to produce PGS-Mg under the same conditions. ICP revealed that the amount of Mg^{2+} in PGSM-Mg was 5.63 ± 0.38 mg g^{-1}, much more than that in PGS-Mg (0.57 ± 0.18 mg g^{-1}) (Fig. 2A), thus indicating that carboxyl groups could immobilize Mg^{2+} effectively. In addition, SEM elemental mapping and EDS semi-quantitative analysis showed that Mg^{2+} on the PGSM-Mg film was more than that on the PGS-Mg film (Fig. 2B and Fig. S2). The characteristic symmetric stretching vibration of the —COO— group at 1438 cm^{-1} in ATR-FTIR spectra indicated the presence of interaction between the carboxyl group and Mg^{2+} (Fig. S3). Moreover, XPS analyses further confirmed the chemical bonding between Mg^{2+} and the carboxyl group. Two peaks were labeled O_1 and O_2 in PGSM and PGSM-Mg spectra, and accordingly, the curve fitting of the O_{1s} peak was associated with different oxygen species: O_1 with oxygen in —O— (532.18 eV) and O_2 with carbonyl oxygen C=O (533.68 eV) (Fig. 2C). The increase in O_2 signal and the simultaneous decrease in O_1 of PGSM-Mg, compared to that in PGSM, revealed the interaction between Mg^{2+} and carboxyl groups.

Thermal properties of PGSM-Mg were investigated by TGA and DSC. PGSM-Mg was stable up to 191 °C (Fig. 2D), while the thermal decomposition temperature of PGS and PGSM was 319 °C (Fig. S4) and 185 °C (Fig. S5), respectively. Because of the introduction of the maleic acid moiety, PGSM-Mg and PGSM exhibited no crystallization from −70 °C to 150 °C compared to the PGS (Fig. S6). The PGSM-Mg had a low T_g of −34.2 °C (Fig. 2D), which was similar to that of PGSM (Fig. S7). PGSM-Mg was in a semisolid state at room temperature and exhibited shear thinning (Fig. S8); thus, it could be used as an injectable material (Fig. 2F). The hydrophilicity of PGSM-Mg was investigated by measuring its static air–water contact angle. As expected, PGSM-Mg had favorable hydrophilicity with a water contact angle of 50.9 ± 2.8°, which is likely due to the introduction of hydrophilic maleic acid groups and Mg^{2+}, as indicated by the relatively higher water contact angles of PGSM (65.1 ± 6.1°) and PGS (80.0 ± 5.2°).

One of the potential applications of PGSM-Mg is to serve as a reservoir for the sustained release of bioactive Mg^{2+}. As shown in Fig. 2G, PGSM-Mg gradually released Mg^{2+} in PBS with a total mass

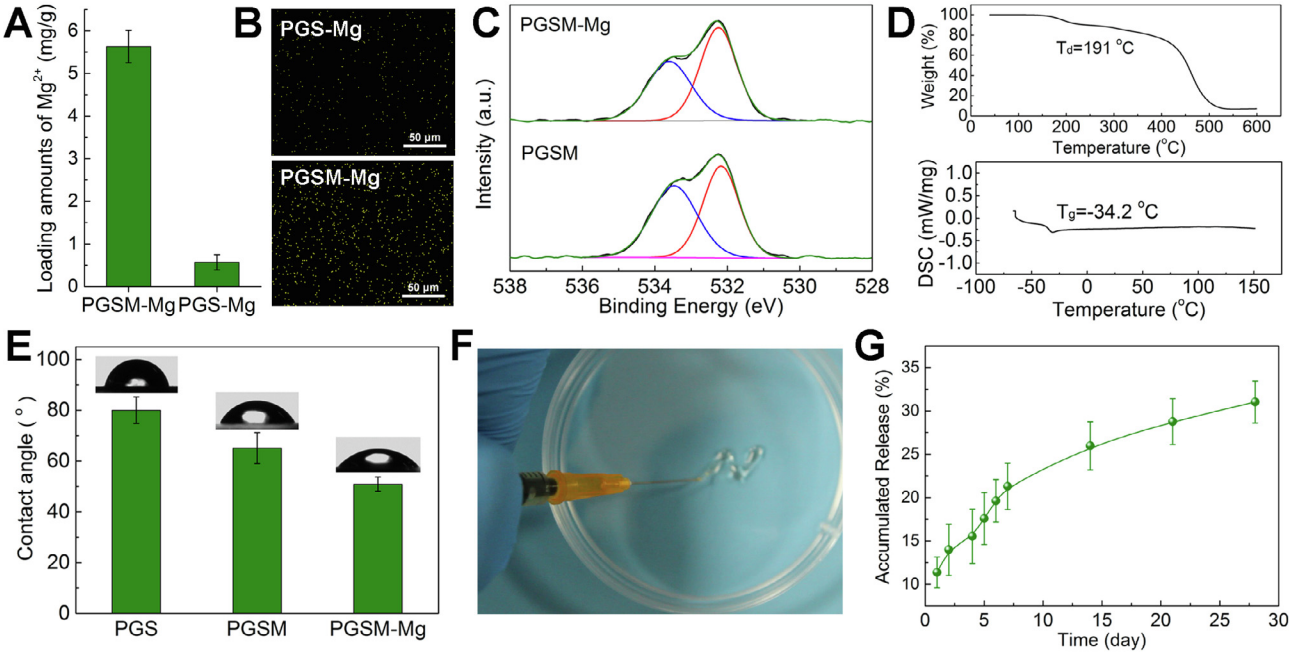

Fig. 2. Characterization of PGSM-Mg: (A) ICP quantitative analysis of the loading amounts of Mg^{2+} on PGSM-Mg and PGS-Mg. (B) Mg elemental mapping of PGS-Mg and PGS-M-Mg film. (C) XPS analyses of PGSM-Mg and PGSM revealed the interaction between carboxyl and Mg^{2+}. (D) TGA and DSC thermograms of PGSM-Mg. (E) Contact angles of PGS, PGSM, and PGSM-Mg. (F) Macroscopic images showed that PGSM-Mg was a viscous semi-solid and could be readily injected. (G) Release profile of Mg^{2+} from the PGSM-Mg film in PBS solution.

loss of 31.0 ± 2.4% during a period of 28 days. This indicated the strong interaction between PGSM and Mg^{2+}, which enabled a long-term release of Mg^{2+}.

3.2. Preparation and characterization of the PGSM-Mg scaffold

PGSM-Mg could be readily processed similar to its precursor polymer PGSM. We used thermal curing and salt leaching methods to fabricate a porous PGSM-Mg 3D scaffold. The impregnated salt template was cured at 150 °C and 1 Torr for 48 h followed by salt leaching and freeze-drying. The morphology of the scaffold was analyzed by SEM (Fig. 3A). Macropores (75–150 μm) controlled by a porogen (salt particles) were well distributed throughout the scaffold and connected to each other, and they had similar porosity (Fig. S9). ICP showed that the cured PGSM-Mg scaffold contained Mg^{2+} of 5.40 ± 0.40 mg g^{-1}, similar to that in the original PGSM-Mg. This revealed Mg^{2+} had adequate compatibility with the harsh processing. Furthermore, elemental mapping of the PGSM-Mg scaffold revealed the uniform spatial distribution of Mg^{2+} along the scaffold (Fig. 3B), thus indicating the efficient incorporation of Mg^{2+} and PGSM at the molecular level.

The TGA of the PGSM-Mg scaffold revealed that it was stable up to 309 °C (Fig. S10). The DSC curve of the PGSM-Mg scaffold showed a T_g of −30.3 °C and no crystallization between −70 °C and 150 °C (Fig. S11), hence indicating its elastic nature at ambient and body environment. The mechanical properties of the PGSM-Mg scaffold were investigated by the compression test (Fig. 3C). The simple compression test revealed that the modulus of the PGSM-Mg scaffold was 4.99 ± 0.83 kPa (Fig. 3D), similar to that of the PGSM scaffold (4.63 ± 0.34 kPa) and slightly higher than that of

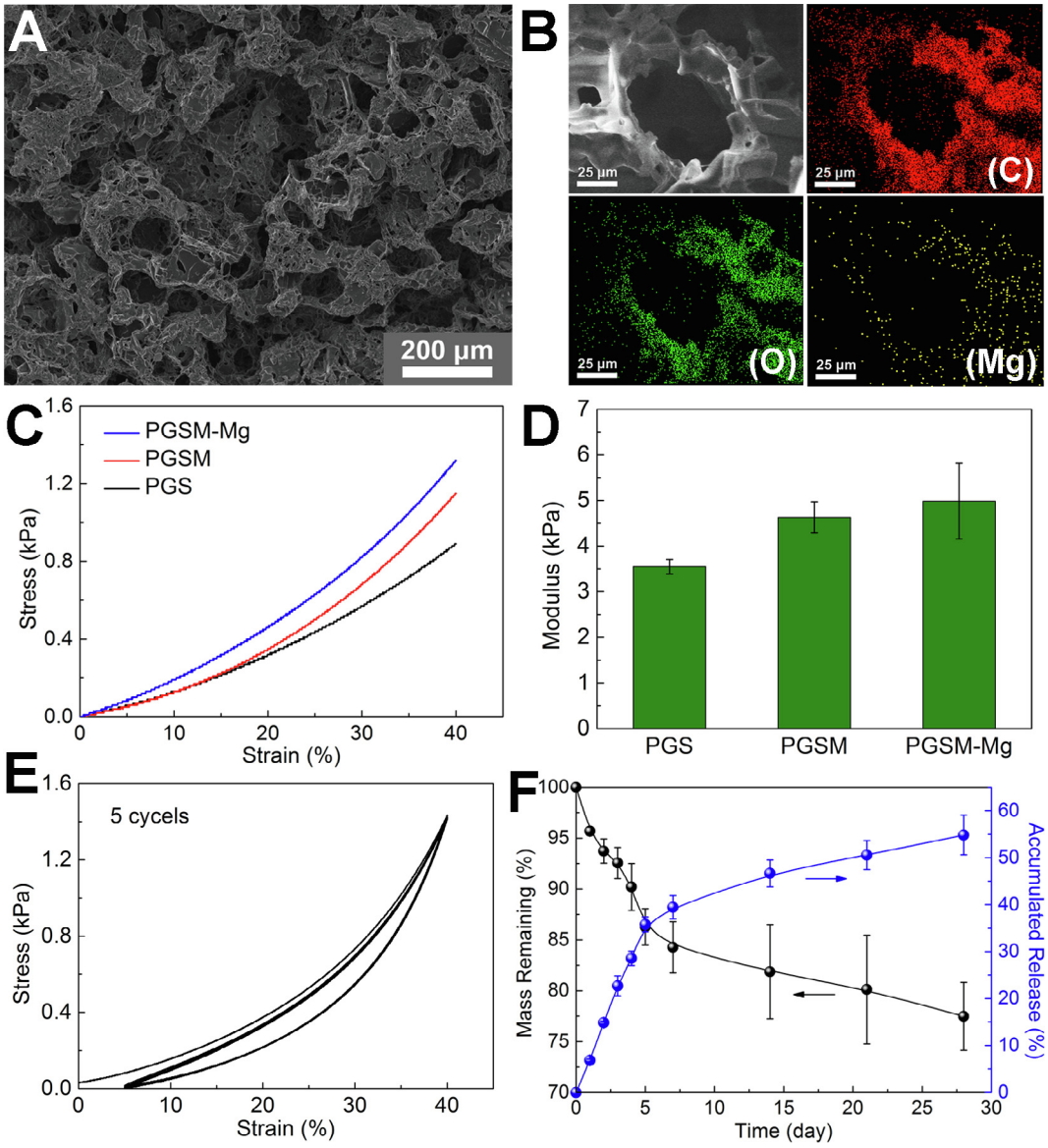

Fig. 3. Characterization of the thermally cured PGSM-Mg porous scaffolds. (A) SEM image of the PGSM-Mg scaffold showed its hierarchical porous structure with interconnected macropores (75–150 μm) derived from porogens (salt particles) and extensive micropores (several microns) throughout the walls of the macropores. This structure was beneficial for cell penetration, cell-to-cell interactions, and mass transport. (B) Representative elemental mapping of the PGSM-Mg scaffold, carbon mapping (red), oxygen mapping (green), and magnesium mapping (yellow) confirmed that the spatial distribution of Mg^{2+} along the scaffold was uniform. (C) Typical stress vs. strain curve of the PGS, PGSM, and PGSM-Mg scaffolds in a uniaxial compression test with a strain up to 40%. (D) Comparison of the moduli of PGS, PGSM, and PGSM-Mg scaffolds, thus indicating the soft nature of the PGSM-Mg scaffold. (E) Typical stress vs. strain curve of the PGSM-Mg scaffold in a cyclic compression test, and a strain up to 40% for 5 cycles revealed adequate elasticity. (F) The PGSM-Mg scaffold degraded gradually in the PBS solution while steadily releasing the Mg2 + . (For interpretation of the references to colour in this figure legend, the reader is referred to the web version of this article.)

the PGS scaffold (3.55 ± 0.16 kPa). Furthermore, cyclic compression test with a strain up to 40% for 5 cycles showed that the PGSM-Mg scaffold could recover well from dynamic deformation (Fig. 3E). These results indicated that the introduction of Mg^{2+} did not have an effect on the soft nature of materials.

The backbone of the PGSM-Mg scaffold is based on ester bonds; hence, it can be degraded by hydrolysis. We investigated the *in vitro* degradation of cured PGSM-Mg scaffolds in PBS solution. The scaffolds gradually degraded with a mass loss of 22.5 ± 3.3% within 28 days (Fig. 3F). It confirmed the adequate biodegradability of PGSM-Mg and indicated the ester groups were likely the primary degradation sites. PGSM-Mg scaffolds well maintained their morphologies during the degradation as observed by SEM images (Fig. S12). With the degradation, PGSM-Mg scaffolds continuously released Mg^{2+}, with an accumulated release amount of 54.8 ± 4.2% within 28 days (Fig. 3F). During the degradation, the pH values kept stable at around 6.5–7 and had little effect on the material degradation process (Fig. S13).

3.3. PGSM-Mg–SC interaction

For the regeneration of injured peripheral nervous system (PNS), SCs play a critical role during this period through a synergetic effect with macrophages and neurons. Therefore, we used SCs as an *in vitro* model to evaluate the cytocompatibility and neuroactivity of PGSM-Mg.

3.3.1. Cell morphology

Phase contrast images were used to investigate cell morphology (Fig. 4A). SCs began to adhere to the PGSM-Mg within 4 days after cell seeding and expanded well, thus displaying a typical fusiform shape. Cell numbers increased 2 to 3 times compared to the initial cell numbers after 6 days postseeding. In addition, cell numbers on the PGSM-Mg film were more than those on PLGA and TCPS films, thus indicating the better cytocompatibility of PGSM-Mg.

3.3.2. Cell proliferation

The CCK-8 assay was used to evaluate the effect of PGSM-Mg on cell proliferation (Fig. 4B). The number of metabolically active SCs on TCPS, PLGA, PGS, PGSM, and PGSM-Mg significantly increased with time. Overall, the number of SCs on PGSM-Mg was similar to the ones on PGS and PGSM during 8 days of culture, while it was significantly higher than the ones on TCPS and PLGA at days 6 and 8 postseeding ($p < 0.05$). This revealed that PGSM-Mg had adequate cytocompatibility with SCs and a stronger ability to promote SC proliferation than TCPS and PLGA.

3.3.3. Expression of neural-specific genes of SCs on PGSM-Mg

RT-qPCR analysis showed that PGSM-Mg could enhance the function of SCs. SCs on PGSM-Mg had the highest gene expression of NGF, which is significantly higher than that in the PLGA group (Fig. 4C).

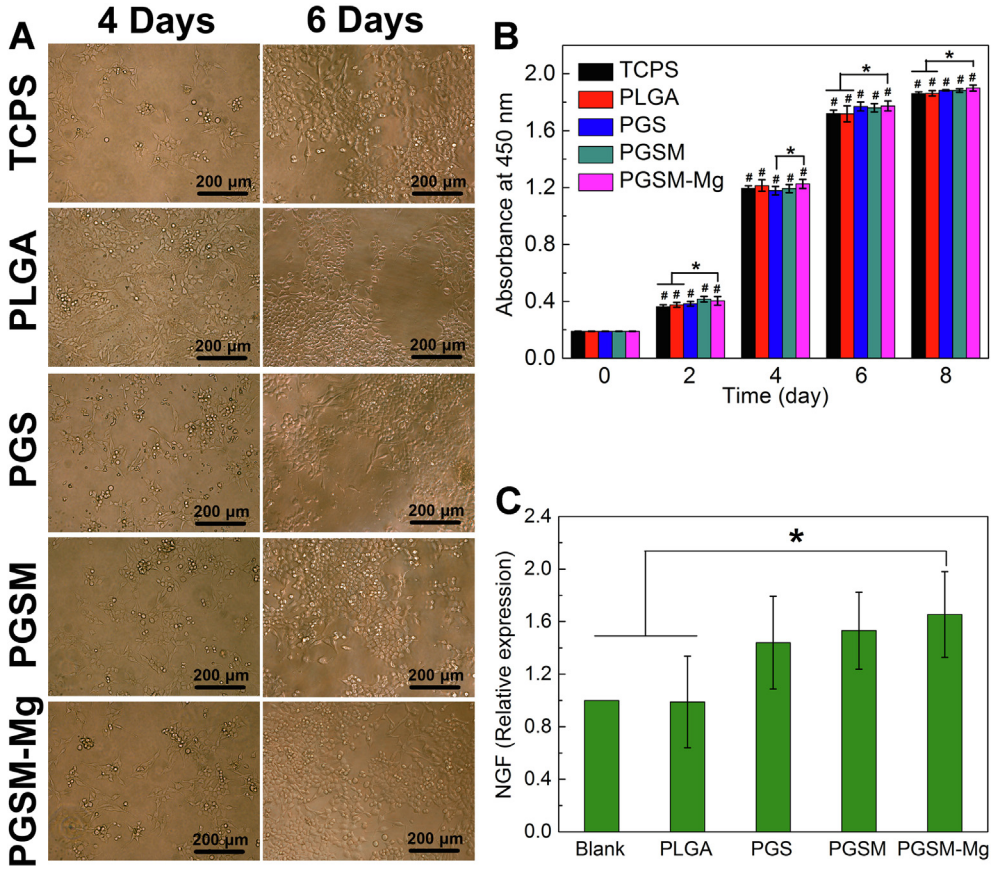

Fig. 4. Biological evaluation of PGSM-Mg (A) Phase- contrast images of SCs on TCPS, PLGA, PGS, PGSM, and PGSM-Mg surfaces at 4 and 6 days after cell seeding showed typical morphology and an increased amount of SCs on all surfaces; (B) CCK-8 assay of SCs cultured on TCPS, PLGA, PGS, PGSM, and PGSM-Mg surfaces. The optical density (OD) value significantly increased in another day within 8 days' of culture and the one on PGSM-Mg surface was higher than that on other surfaces after 4 days' of culture. These results revealed that PGSM-Mg promoted the proliferation of SCs better than its non-metallic counterparts (PGSM and PGS) and standard culture substrates (PLGA and TCPS). (C) Neural-specific gene expression of NGF for SCs cultured on TCPS, PLGA, PGS, PGSM, and PGSM-Mg surfaces after 6 days. The SCs on PGSM-Mg showed the highest gene expression of NGF, which was significantly higher than that in the PLGA group.

3.4. PGSM-Mg scaffold–SC interaction

3.4.1. Cell proliferation on 3D scaffolds

The CCK-8 assay was used to evaluate the effect of PGSM-Mg scaffolds on cell proliferation (Fig. 5A). The number of metabolically active SCs on PLGA, PGS, PGSM, and PGSM-Mg scaffolds significantly increased with time in the culture. The number of SCs on the PGSM-Mg scaffold was significantly higher than those on PGS, PGSM, and PLGA scaffolds at days 4 and 6 postseeding ($p < 0.05$). These results indicated that the PGSM-Mg scaffold had adequate cytocompatibility with SCs and a stronger ability to promote SCs proliferation than PLGA. The image of live cells at day 8 revealed the wide distribution of SCs throughout the scaffolds, thus indicating the scaffolds provided an instructive 3D niche for cells (Fig. S14).

3.4.2. Cell morphology on 3D scaffolds

After 8 days of culture, SCs on scaffolds were fixed and investigated by SEM (Fig. 5B). SCs on PLGA, PGS, PGSM, and PGSM-Mg scaffolds showed similar morphology. Part of SCs on PGSM-Mg exhibited a typical flat and slender shape with bulged center, thus indicating PGSM-Mg was a favorable substrate for SC culture.

3.4.3. Expression of neural-specific genes of SCs on PGSM-Mg scaffolds

RT-qPCR analysis showed that PGSM-Mg scaffolds could enhance the function of SCs. The SCs on PGSM-Mg scaffolds had the most significantly enhanced neural-specific gene expression of NGF (Fig. 5C) compared to those in the other groups. Similarly, the SCs on PGSM-Mg scaffolds showed similarly enhanced

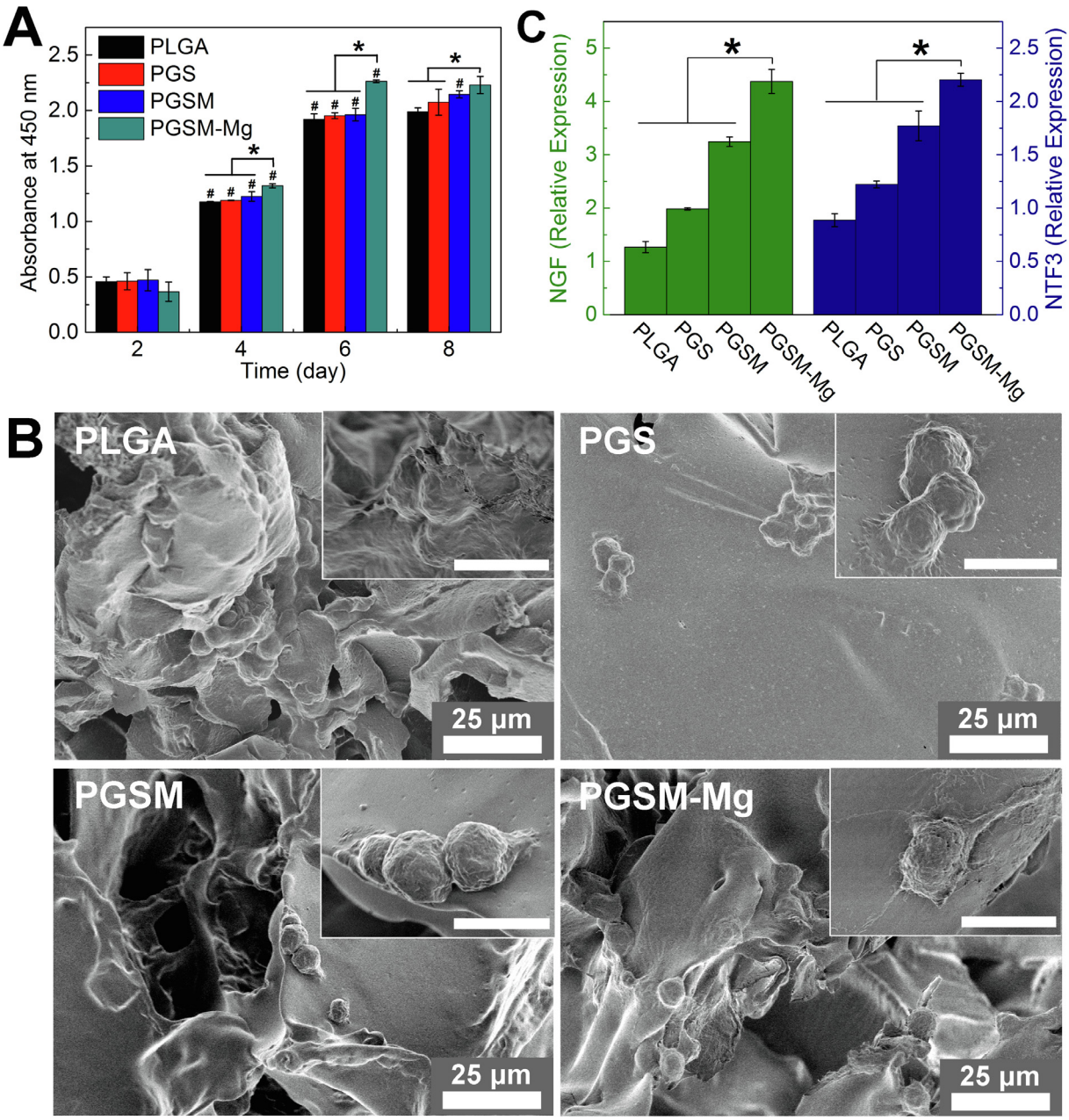

Fig. 5. (A) CCK-8 assay of SCs cultured on PLGA, PGS, PGSM, and PGSM-Mg 3D scaffolds. SCs on PGSM-Mg scaffolds significantly proliferated another day, thus leading to higher amounts than the ones on all other surfaces after 4 days and 6 days. (B) SEM images of SCs on PLGA, PGS, PGSM, and PGSM-Mg scaffolds after 8 days *in vitro* culture. The inset showed the magnified images of cell morphology (scale bar = 5 μm). (C) NGF and NTF3 expression of SCs cultured on PLGA, PGS, PGSM, and PGSM-Mg scaffolds after 6 days. PGSM-Mg efficiently enhanced neural-specific gene expression of NGF and NTF3. *: Statistically significant difference between different materials at the same time point ($p < 0.05$).

neural-specific gene expression of NTF3 compared to those on PGS and higher than those on PGSM (Fig. 5C).

4. Discussion

In this study, we designed a new neuroactive polymer with Mg^{2+}, PGSM-Mg. PGSM-Mg significantly enhanced the proliferation and neural-specific gene expression of SCs compared to PLGA, PGS and PGSM. At the same time, PGSM-Mg is a soft material with a desirable injectability and can be used to construct a 3D elastic scaffold. The compression modulus of the PGSM-Mg scaffold was similar to that of the PGS scaffold, which is favorable to cells of soft tissues [36].

Herein, a simple, general, and effective approach was developed to construct novel bioactive soft biomaterials by hybridizing metal ions and polymers at the molecular level. Particularly, we developed the neuroactive polymer PGSM-Mg. As the backbone of PGSM-Mg, PGS has excellent biocompatibility, elasticity, and biodegradability and thus has been widely used for various biomedical applications including tissue engineering [2,3], drug delivery [37,38], and biosensors [39,40]. However, the absence of bioactivity limits further application of PGS. Some efforts have been employed to enhance its bioactivity. Introducing biomacromolecules such as proteins into PGS presented a typical way by using different processing methods such as coating, blending, and covalent bonding. However, physical interaction is unstable and may cause the denaturation of biomaterials. Recently, we integrated small bioactive molecules with newly regenerated PGS – poly(sebacoyl diglyceride) – to produce osteoconductive and neuroactive biomaterials [34,41]. However, these materials suffered from complex synthetic processes. This study aimed to use metal ions as a new, simple, and effective approach to endow polymers with suitable bioactivities taking PGS and Mg^{2+} as an example. However, it was difficult to integrate PGS with metal ions directly owing to the lack of strong interaction with metal ions (Fig. 2A). Herein, we introduced carboxyl groups to PGS side chain (PGSM) through a biocompatible maleate unit to serve as binding sites to the metal ion. Carboxyl is widely distributed in living organisms and one of the most common groups to bind metal ions in the body. PGSM had desirable biocompatibility (Fig. 4A–B), while it could significantly promote the the production of NGF and NTF3 by SCs (Fig. 5C), which finding was consistent with the findings in previous reports [42]. Preimmobilized cations (such as Mg^{2+}, Mn^{2+}, or Ca^{2+} ions) in materials as bioactive cell recognition moieties and integrin receptors can mediate diverse cell–material interactions such as cell adhesion and differentiation [43,44]. For example, it was reported that the incorporation of Mg^{2+} moieties in the material could effectively induce integrin binding and specific gene expression. The content of Mg^{2+} in resultant PGSM-Mg increased to 5.63 ± 0.38 mg g^{-1}, which is approximately 10 times of the one in PGS-Mg (0.57 ± 0.18 mg g^{-1}), thus revealing that carboxyl groups did immobilize Mg^{2+} effectively. SEM mapping and XPS analysis further confirmed the interaction between PGSM and Mg^{2+} (Fig. 2B-C). Moreover, cured PGSM-Mg porous scaffolds synthesized under harsh conditions (150 °C, 1 Torr) kept a similar content and uniform distribution of Mg^{2+}. Both PGSM-Mg film and cured PGSM-Mg scaffold maintained a sustained release of Mg^{2+} during degradation. Compared to a two-dimensional film, the highly porous scaffold has a larger specific surface area leading to the faster release of Mg^{2+}. SC culture demonstrated the neuroactivity of PGSM-Mg, especially the corresponding scaffold, because the scaffold could provide 3D culturing microenvironments to better mimic the extracellular matrix. These results demonstrated the introduction of Mg^{2+} did endow the neuroactivity to the polymer and the neuroactivity of Mg^{2+} could be well retained under harsh conditions. In addition to neuroactivity, Mg^{2+} has other biological functions such as cartilage activity [20,44]. To the best of our knowledge, this is the first report on bioactive Mg^{2+}/polymer hybrid. In view of the stability and easy denaturing of other bioactive factors such as proteins and genes, incorporation of metal ions provides a new alternative practical way to construct bioactive polymers.

It is worthy to note that PGSM-Mg hybrid well retains the soft nature and facile processing ability of the polymer precursor PGSM. Previous studies on metal ion-containing materials are usually inorganic ones, which are hard and do not match the mechanical properties of soft tissues. In contrast, PGSM-Mg is a soft semisolid at room temperature (Fig. 2F), could be readily processed as typical pure polymers, and even used as an injectable material. Injectable materials can be implanted by minimally invasive approaches and fill any shape, which is able to decrease the surgery time and additional trauma to the tissue around the implant site. PGSM-Mg can be used as a reservoir of Mg^{2+} and mixed with hydrophobic drugs as a drug delivery vehicle [45]. Furthermore, salt leaching method combing with thermal curing produced porous PGSM-Mg scaffolds with an excellent elasticity (Fig. 3E). Because of the small amount of Mg^{2+}, the PGSM-Mg scaffold retained the soft nature and similar elastic modulus of the PGS and PGSM scaffolds, which was distinct from brittle inorganic materials and favorable for soft tissue applications.

The strategy on creating neuroactive PGSM-Mg is general. Plenty of polymers contain carboxyl groups. The carboxyl groups can be used to bind a wide range of metal ions including Mg^{2+}, copper ion (Cu^{2+}), and calcium ion (Ca^{2+}). Moreover, we can use other organic functional groups such as imidazole, catechol, and pyridine as bridges to integrate metal ions and polymers. Accordingly, more diverse metal ions can be used and will elicit different biological functions suitable for different tissue regeneration. Furthermore, by varying the structures of backbone polymers, the physical, chemical, and mechanical properties of the hybrid materials can be modulated to fulfill the requirements for different tissues. Accordingly, this strategy can construct a series of new metal ion/polymer hybrids as new potential biomaterials. Systematical evaluation of these new hybrid materials including their various properties, interactions with cells, and *in vivo* performance will be conducted in the future.

5. Conclusions

We propose a new design principle to construct bioactive soft materials by molecularly integration of metal ions and polymers. We demonstrated the efficiency of this principle by developing a new neuroactive hybrid material, PGSM-Mg. PGSM-Mg exhibits similar physical, mechanical, and processing properties as those of its polymer precursor PGSM. Mg^{2+} was uniformly distributed throughout the material and gradually released during material degradation. PGSM-Mg promoted the adhesion, proliferation, and neural-specific gene expression of SCs. The design principle is general, and synthetic route is versatile, which can be readily applied to other metal ions and polymers. We expected this work will pave a new way to construct bioactive soft materials for a wide range of biomedical applications.

Acknowledgments

The authors highly appreciate Dr. Yadong Wang from Cornell University for the instructive discussion and manuscript editing. This work was financially supported by the Natural Science Foundation of Shanghai (18ZR1401900), the International Joint Laboratory for Advanced Fiber and Low-dimension Materials

(18520750400), the National Natural Science Foundation of China (21574019, 31570984, and 31771023), and the Science and Technology Commission of Shanghai (17DZ2260100).

Disclosures

The authors have no competing interests to declare.

Appendix A. Supplementary data

Supplementary data to this article can be found online at https://doi.org/10.1016/j.actbio.2018.12.040.

References

[1] G.S. Hussey, J.L. Dziki, S.F. Badylak, Extracellular matrix-based materials for regenerative medicine, Nat. Rev. Mater. 3 (7) (2018) 159–173.
[2] H. Ye, K. Zhang, D. Kai, Z. Li, X.J. Loh, Polyester elastomers for soft tissue engineering, Chem. Soc. Rev. 47 (12) (2018) 4545–4580.
[3] Q. Chen, S. Liang, G.A. Thouas, Elastomeric biomaterials for tissue engineering, Prog. Polym. Sci. 38 (3–4) (2013) 584–671.
[4] S.R. Meyers, M.W. Grinstaff, Biocompatible and bioactive surface modifications for prolonged in vivo efficacy, Chem. Rev. 112 (3) (2012) 1615–1632.
[5] T. Zhou, Y. Zhu, X. Li, X. Liu, K.W.K. Yeung, S. Wu, X. Wang, Z. Cui, X. Yang, P.K. Chu, Surface functionalization of biomaterials by radical polymerization, Prog. Mater. Sci. 83 (2016) 191–235.
[6] R. Rai, M. Tallawi, C. Frati, A. Falco, A. Gervasi, F. Quaini, J.A. Roether, T. Hochburger, D.W. Schubert, L. Seik, N. Barbani, L. Lazzeri, E. Rosellini, A.R. Boccaccini, Bioactive electrospun fibers of poly(glycerol sebacate) and poly (epsilon-caprolactone) for cardiac patch application, Adv. Healthcare Mater. 4 (13) (2015) 2012–2025.
[7] A. Gao, R. Hang, W. Li, W. Zhang, P. Li, G. Wang, L. Bai, X.F. Yu, H. Wang, L. Tong, P.K. Chu, Linker-free covalent immobilization of heparin, SDF-1alpha, and CD47 on PTFE surface for antithrombogenicity, endothelialization and anti-inflammation, Biomaterials 140 (2017) 201–211.
[8] A. Harguindey, D.W. Domaille, B.D. Fairbanks, J. Wagner, C.N. Bowman, J.N. Cha, Synthesis and assembly of click-nucleic-acid-containing PEG-PLGA nanoparticles for DNA delivery, Adv. Mater. 29 (24) (2017) 1700743.
[9] C. Wang, L. Du, J. Zhou, L. Meng, Q. Cheng, C. Wang, X. Wang, D. Zhao, Y. Huang, S. Zheng, H. Cao, J. Zhang, L. Deng, Z. Liang, A. Dong, Elaboration on the distribution of hydrophobic segments in the chains of amphiphilic cationic polymers for small interfering RNA delivery, ACS Appl. Mater. Interfaces 9 (38) (2017) 32463–32474.
[10] L. Zhu, K. Wang, T. Ma, L. Huang, B. Xia, S. Zhu, Y. Yang, Z. Liu, X. Quan, K. Luo, Noncovalent bonding of RGD and YIGSR to an electrospun poly(ε-Caprolactone) conduit through peptide self-assembly to synergistically promote sciatic nerve regeneration in rats, Adv. Healthcare Mater. 6 (8) (2017) 1600860.
[11] S. Li, Y. Xu, J. Yu, M.L. Becker, Enhanced osteogenic activity of poly(ester urea) scaffolds using facile post-3D printing peptide functionalization strategies, Biomaterials 141 (2017) 176–187.
[12] U. Grober, J. Schmidt, K. Kisters, Magnesium in prevention and therapy, Nutrients 7 (9) (2015) 8199–8226.
[13] H. Kozlowski, S. Potocki, M. Remelli, M. Rowinska-Zyrek, D. Valensin, Specific metal ion binding sites in unstructured regions of proteins, Coord. Chem. Rev. 257 (19–20) (2013) 2625–2638.
[14] C.C. Correll, B. Freeborn, P.B. Moore, T.A. Steitz, Metals, motifs, and recognition in the crystal structure of a 5S rRNA domain, Cell 91 (5) (1997) 705–712.
[15] C. Wu, Y. Zhou, M. Xu, P. Han, L. Chen, J. Chang, Y. Xiao, Copper-containing mesoporous bioactive glass scaffolds with multifunctional properties of angiogenesis capacity, osteostimulation and antibacterial activity, Biomaterials 34 (2) (2013) 422–433.
[16] C. Wu, Y. Zhou, C. Lin, J. Chang, Y. Xiao, Strontium-containing mesoporous bioactive glass scaffolds with improved osteogenic/cementogenic differentiation of periodontal ligament cells for periodontal tissue engineering, Acta Biomater. 8 (10) (2012) 3805–3815.
[17] C. Wu, Y. Zhou, W. Fan, P. Han, J. Chang, J. Yuen, M. Zhang, Y. Xiao, Hypoxia-mimicking mesoporous bioactive glass scaffolds with controllable cobalt ion release for bone tissue engineering, Biomaterials 33 (7) (2012) 2076–2085.
[18] Y. Lu, L. Li, Y. Zhu, X. Wang, M. Li, Z. Lin, X. Hu, Y. Zhang, Q. Yin, H. Xia, C. Mao, Multifunctional copper-containing carboxymethyl chitosan/alginate scaffolds for eradicating clinical bacterial infection and promoting bone formation, ACS Appl. Mater. Interfaces 10 (1) (2018) 127–138.
[19] C. Wu, L. Xia, P. Han, L. Mao, J. Wang, D. Zhai, B. Fang, J. Chang, Y. Xiao, Europium-containing mesoporous bioactive glass scaffolds for stimulating in vitro and in vivo osteogenesis, ACS Appl. Mater. Interfaces 8 (18) (2016) 11342–11354.
[20] A. Hoppe, N.S. Guldal, A.R. Boccaccini, A review of the biological response to ionic dissolution products from bioactive glasses and glass-ceramics, Biomaterials 32 (11) (2011) 2757–2774.
[21] K. Zheng, J. Wu, W. Li, D. Dippold, Y. Wan, A.R. Boccaccini, Incorporation of Cu-containing bioactive glass nanoparticles in gelatin-coated scaffolds enhances bioactivity and osteogenic activity, ACS Biomater. Sci. Eng. 4 (5) (2018) 1546–1557.
[22] J. Bejarano, R. Detsch, A.R. Boccaccini, H. Palza, PDLLA scaffolds with Cu- and Zn-doped bioactive glasses having multifunctional properties for bone regeneration, J. Biomed. Mater. Res. A 105 (3) (2017) 746–756.
[23] S. D'Mello, S. Elangovan, L. Hong, R.D. Ross, D.R. Sumner, A.K. Salem, Incorporation of copper into chitosan scaffolds promotes bone regeneration in rat calvarial defects, J. Biomed. Mater. Res. B 103 (5) (2015) 1044–1049.
[24] M. Frydrych, S. Roman, S. MacNeil, B. Chen, Biomimetic poly(glycerol sebacate)/poly(l-lactic acid) blend scaffolds for adipose tissue engineering, Acta Biomater. 18 (2015) 40–49.
[25] X.F. Ye, L. Lu, M.E. Kolewe, K. Hearon, K.M. Fischer, J. Coppeta, L.E. Freed, Scalable units for building cardiac tissue, Adv. Mater. 26 (42) (2014) 7202–7208.
[26] C.N. Hsu, P.Y. Lee, H.Y. Tuan-Mu, C.Y. Li, J.J. Hu, Fabrication of a mechanically anisotropic poly(glycerol sebacate) membrane for tissue engineering, J. Biomed. Mater. Res. B 106 (2) (2018) 760–770.
[27] R.A. Allen, W. Wu, M. Yao, D. Dutta, X. Duan, T.N. Bachman, H.C. Champion, D. B. Stolz, A.M. Robertson, K. Kim, J.S. Isenberg, Y. Wang, Nerve regeneration and elastin formation within poly(glycerol sebacate)-based synthetic arterial grafts one-year post-implantation in a rat model, Biomaterials 35 (1) (2014) 165–173.
[28] Y. Wu, L. Wang, B. Guo, Y. Shao, P.X. Ma, Electroactive biodegradable polyurethane significantly enhanced Schwann cells myelin gene expression and neurotrophin secretion for peripheral nerve tissue engineering, Biomaterials 87 (2016) 18–31.
[29] Y.D. Wang, G.A. Ameer, B.J. Sheppard, R. Langer, A tough biodegradable elastomer, Nat. Biotechnol. 20 (6) (2002) 602–606.
[30] H.C. Pan, M.L. Sheu, H.L. Su, Y.J. Chen, C.J. Chen, D.Y. Yang, W.T. Chiu, F.C. Cheng, Magnesium supplement promotes sciatic nerve regeneration and down-regulates inflammatory response, Magnes. Res. 24 (2) (2011) 54–70.
[31] J. Fei, X. Wen, X. Lin, W. Saijilafu, O. Wang, X. Ren, L. Chen, K. Tan, H. Yang, L. Yang, Biocompatibility and neurotoxicity of magnesium alloys potentially used for neural repairs, Mater. Sci. Eng. C 78 (2017) 1155–1163.
[32] B.H. Li, K. Yang, X. Wang, Biodegradable magnesium wire promotes regeneration of compressed sciatic nerves, Neural Regen. Res. 11 (12) (2016) 2012–2017.
[33] Z. You, X. Bi, X. Fan, Y. Wang, A functional polymer designed for bone tissue engineering, Acta Biomater. 8 (2) (2012) 502–510.
[34] P. Huang, X. Bi, J. Gao, L. Sun, S. Wang, S. Chen, X. Fan, Z. You, Y. Wang, Phosphorylated poly (sebacoyl diglyceride)–a phosphate functionalized biodegradable polymer for bone tissue engineering, J. Mater. Chem. B 4 (12) (2016) 2090–2101.
[35] X. Deng, M. Paven, P. Papadopoulos, M. Ye, S. Wu, T. Schuster, M. Klapper, D. Vollmer, H.J. Butt, Solvent-free synthesis of microparticles on superamphiphobic surfaces, Angew. Chem. Int. Ed. 52 (43) (2013) 11286–11289.
[36] J. Gao, P.M. Crapo, Y. Wang, Macroporous elastomeric scaffolds with extensive micropores for soft tissue engineering, Tissue Eng. 12 (4) (2006) 917–925.
[37] B. Louage, L. Tack, Y. Wang, B.G. De Geest, Poly(glycerol sebacate) nanoparticles for encapsulation of hydrophobic anti-cancer drugs, Polym. Chem. 8 (34) (2017) 5033–5038.
[38] C. Zhu, A.E. Rodda, V.X. Truong, Y. Shi, K. Zhou, J.M. Haynes, B. Wang, W.D. Cook, J.S. Forsythe, Increased cardiomyocyte alignment and intracellular calcium transients using micropatterned and drug-releasing poly(glycerol sebacate) elastomers, ACS Biomater. Sci. Eng. 4 (7) (2018) 2494–2504.
[39] Y.J. Kim, S.-E. Chun, J. Whitacre, C.J. Bettinger, Self-deployable current sources fabricated from edible materials, J. Mater. Chem. B 1 (31) (2013) 3781–3788.
[40] C.M. Boutry, A. Nguyen, Q.O. Lawal, A. Chortos, S. Rondeau-Gagne, Z. Bao, A sensitive and biodegradable pressure sensor array for cardiovascular monitoring, Adv. Mater. 27 (43) (2015) 6954–6961.
[41] S. Wang, E. Jeffries, J. Gao, L. Sun, Z. You, Y. Wang, Polyester with pendent acetylcholine-mimicking functionalities promotes neurite growth, ACS Appl. Mater. Interfaces 8 (15) (2016) 9590–9599.
[42] Y. Wang, Y. Ji, Y. Zhao, Y. Kong, M. Gao, Q. Feng, Y. Wu, Y. Yang, Effects of surface functional groups on proliferation and biofunction of Schwann cells, J. Biomater. Appl. 30 (10) (2016) 1494–1504.
[43] H. Kang, K. Zhang, H.J. Jung, B. Yang, X. Chen, Q. Pan, R. Li, X. Xu, G. Li, V.P. Dravid, L. Bian, An in situ reversible heterodimeric nanoswitch controlled by metal-ion-ligand coordination regulates the mechanosensing and differentiation of stem cells, Adv. Mater. 30 (44) (2018) 1803591.
[44] H. Zreiqat, C.R. Howlett, A. Zannettino, P. Evans, G. Schulze-Tanzil, C. Knabe, M. Shakibaei, Mechanisms of magnesium-stimulated adhesion of osteoblastic cells to commonly used orthopaedic implants, J. Biomed. Mater. Res. 62 (2) (2002) 175–184.
[45] M. Tran, C. Wang, Semi-solid materials for controlled release drug formulation: current status and future prospects, Front. Chem. Sci. Eng. 8 (2) (2014) 225–232.